

# Experimental observation of laser-induced coherent ion motion in a quadrupole trap

Jos Oomens<sup>a,\*</sup>, Gert von Helden<sup>a</sup>, Gerard Meijer<sup>a,b,c</sup>

<sup>a</sup> FOM Institute for Plasma Physics “Rijnhuizen”, Edisonbaan 14, 3439MN Nieuwegein, The Netherlands

<sup>b</sup> Department of Molecular and Laser Physics, University of Nijmegen, Toernooiveld 1, 6525ED Nijmegen, The Netherlands

<sup>c</sup> Department of Molecular Physics, Fritz Haber Institute of the Max Planck Society, Faradayweg 4-6, D-14195 Berlin, Germany

Received 29 August 2002; accepted 23 September 2002

## Abstract

When extracting ions from a quadrupole ion trap into a time-of-flight (TOF) mass spectrometer, oscillations are observed in the intensity and arrival time of the mass-selected ions as a function of the time delay between laser induced ion creation and extraction. The oscillation frequency is inversely proportional to the ion mass, suggesting that the effect is caused by the secular motion of the ions. Based on trajectory simulations, we show that the oscillations are likely due to an asymmetric distribution of initial positions and velocities in phase space, which is caused by the partial overlap between ion cloud and laser beam. Subsequently, this non-perfectly matched phase-space distribution evolves coherently. This is shown to give rise to oscillations in the ion signal at twice the secular frequency, in agreement with observations. (Int J Mass Spectrom 221 (2002) 163–176) © 2002 Elsevier Science B.V. All rights reserved.

**Keywords:** Quadrupole ion trap; Trajectory simulations; Coherent motion; Phase-space dynamics

## 1. Introduction

In a quadrupole ion trap [1], ion motion consists of a fast micromotion at the frequency of the driving rf field and of a much slower secular motion [2–4]. It is known that coherences may occur in the ion cloud motion, which may influence observable ion signals, and therefore, knowledge of this collective motion may be essential, especially when using the trap in collision free mode and/or for time resolved studies.

For a bunch of trapped ions, it is no surprise that the micromotion is coherent, since all ions move in

phase with the driving rf field. However, the situation is less straightforward for the secular motion. Over the past decade, several experimental studies have revealed the existence of various types of coherent secular ion motion [3,5–8]. In addition, trajectory simulation studies have attributed substantially to a detailed understanding of the motion of trapped ions [3,9–11]. Coherent secular ion motion induced by the application of a pulsed laser to the trapped ion cloud, where the ion cloud size is larger than the laser spot size, is the subject of this paper.

Some manifestations of coherent secular motion are well-known to ion trappers. For instance, in the mass-selective instability scan of an ion trap mass spectrometer, use is made of the coherent ejection

\* Corresponding author. E-mails: joso@rijnh.nl, gertvh@rijnh.nl, gerardm@rijnh.nl

of all ions of a specific mass as a function of the rf amplitude [3]. Also, the application of a small ac voltage to the endcap electrodes at the secular frequency is known to cause mass-selective coherent excitation of ion trajectories [3,8,12,13]. Non-destructive mass analysis based on Fourier transformation of the real-time image current, commonly used in ICR traps [14] but also in quadrupole traps [15], relies on this type of coherent ion motion.

In order to map the ion distribution as a function of various trap parameters, Cooks and coworkers developed various ion tomography techniques, based on UV laser photodissociation [5,12,16] as well as on applying a phase-locked dc pulse to one of the endcaps [8,13]. Moreover, since both the laser pulse as well as the dc pulse are locked to the rf-phase and can be applied with sub-microseconds precision, these techniques are well suited to track the ion cloud motion. Thus, coherent ion motion after applying a dipolar ac pulse, resonant with the axial secular frequency, to the endcaps of the trap has been observed [8]. Moreover, it was shown that a quadrupolar dc pulse, i.e., applied to both endcaps simultaneously, squeezes the ion cloud in the axial direction while it blows up in the radial plane [5]. Subsequently, coherent secular motion in the radial direction was observed. It should also be mentioned that these effects were confirmed by detailed trajectory simulations using the ITSIM computer program [9].

These experiments were performed in a quadrupole ion trap that is not only used as storage device but moreover as mass spectrometer, using the mass selective instability scan method. In the following we will focus on instruments that combine an ion trap with a time-of-flight (TOF) spectrometer for mass analysis, as described in Ref. [17].

In an experiment where a neutral supersonic molecular beam was coupled into an ion trap, in the center of which photoionization was applied, Grottemeyer and coworkers reported oscillations in the kinetic energy and flight time of the ions at the secular frequency [6,7]. The oscillations were attributed to the sharply peaked velocity distribution of the molecular beam, which determines the initial conditions of the ion tra-

jectories in the trap, so that the motion of the entire ion bunch behaves as if it were a single ion. It was stated that “when an effusive beam is used instead of a supersonic beam, the time dependence of the ion signals is no longer observed” [6].

In contrast, we will report here on the observation of oscillations in the extraction efficiency and the flight time in an ion trap-TOF instrument starting from vapor phase molecules with random velocity. However, we will also show that these oscillations must be explained by a different mechanism than those reported in Refs. [6–8].

The observations can be conveniently explained using the concept of phase space, where a particle’s velocity is evaluated vs. its position (see Fig. 1). Although the true quadrupolar potential is time dependent, which complicates a description in terms of phase space, ion trajectories can under certain circumstances be described by a time-independent pseudo-potential. In an ideal quadrupole trap, the pseudo-potential is perfectly harmonic, which forces the individual ions to move along elliptic iso-energetic paths in phase space, indicated by the circles in

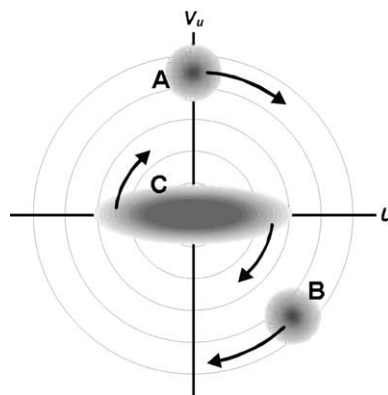


Fig. 1. Phase-space plot along one of the Cartesian coordinates. With the proper scaling of horizontal and vertical axes, the concentric circles represent iso-energetic paths. Different initial ion distributions in phase space give rise to oscillations in observable ion signals. The different initial conditions sketched here represent those of Ref. [6,7] (A), of Ref. [8] (B) and of our experiments as well as those of Ref. [5] (C). The former two processes are classified as “bouncing” whereas the latter distribution yields a “breathing” motion.

Fig. 1.<sup>1</sup> Therefore, creating an off-center distribution in the velocity coordinate as in the experiments of Grottemeyer and coworkers [6,7] (A in Fig. 1), or at a random phase angle as in the experiments of Weil et al. [8] (B in Fig. 1), causes the ion cloud to subsequently circle through phase space. These types of motion are both referred to as “bouncing.”

The oscillations following pulsed laser dissociation as described in this work, are due to a different kind of coherent ion cloud evolution. Via trajectory simulations, we show that it can be understood as being due to the ion cloud “breathing,” i.e., an on-axis but non-uniform ion packet is created in phase space, which, under the influence of the harmonic potential starts to rotate in phase space. This “breathing” motion is depicted by ion cloud C in Fig. 1 and can be regarded as all ions having maximum velocity *spread* and minimum position *spread* at the same time, and vice versa. Cleven et al. [5] showed that a quadrupolar pulse applied to the endcaps of the trap can lead to a similar coherent motion. Here, we describe how this coherent motion is induced by laser interaction and the effects it has on experimentally observable parameters such as extraction efficiency and flight time, and we show that there is good qualitative agreement between observations and trajectory simulations. Finally, it may be noted from the pictorial representation in Fig. 1, that both bouncing and breathing effects vanish when the ion cloud exactly fills up an iso-energetic curve. This concept is known in accelerator physics as beam or phase-space matching [18].

## 2. Theory

In the ion trap, the ions move along complex three-dimensional trajectories with a general appearance of Lissajous’ figures, which are determined by the ions mass-to-charge ratio ( $m/e$ ), the rf frequency ( $\Omega$ ) and amplitude ( $V_{0-p}$ ), and the trap dimension ( $r_0$ ). There

are several textbooks and review papers discussing details of ion motion in the trap (see, e.g., Refs. [2–4]) and therefore we restrict ourselves here to a brief overview of the concepts relevant to the present study.

When there is no dc potential between ring and endcap electrodes ( $U = 0$ ), the three independent differential equations describing the ion trajectories in the quadrupolar potential take the form

$$\begin{aligned} \frac{d^2x}{dt^2} &= -\frac{ex}{mr_0^2} V_{0-p} \cos \Omega t \\ \frac{d^2y}{dt^2} &= -\frac{ey}{mr_0^2} V_{0-p} \cos \Omega t \\ \frac{d^2z}{dt^2} &= \frac{2ez}{mr_0^2} V_{0-p} \cos \Omega t \end{aligned} \quad (1)$$

which are an example of the Mathieu equation [2]. This equation has solutions in the form of superpositions of sine and cosine functions at angular frequencies  $\omega_n = (2n + \beta)\Omega/2$ , where  $\beta$  determines the frequency spectrum corresponding to the pair of Mathieu stability parameters [2]:

$$\begin{aligned} q_z(-2q_r) &= -\frac{4eV_{0-p}}{mr_0^2\Omega^2} \\ a_z(-2a_r) &= -\frac{8eU}{mr_0^2\Omega^2} \end{aligned} \quad (2)$$

for axial ( $z$ ) and radial ( $r$ ) motion. It can be shown that for small values of  $q_z$  (i.e.,  $\leq 0.4$ ), the  $n \neq 0$  terms in the expansion possess negligible amplitudes, so that the oscillatory motion is dominated by the ‘secular’ frequency:

$$\omega_0 = \frac{1}{2}\beta\Omega \quad (3)$$

Moreover, for low values of  $q_z$  one finds  $\beta_z \approx 2\beta_r$  so that secular frequencies in radial and axial directions differ by a factor of 2,  $\omega_{0z} \approx 2\omega_{0r}$ .

To determine the secular frequency  $\omega_0$ , the value of  $\beta$  can be estimated using an iterative procedure involving the stability  $a$  and  $q$  parameters [3]. However, the secular frequency can also be determined applying the pseudo-potential method [2,19], which is valid roughly for  $q_z \leq 0.4$ . This adiabatic approximation uncouples the low-frequency large-amplitude

<sup>1</sup> In a perfect quadrupolar potential (as we will consider throughout this work), the motions in  $x$ -,  $y$ - and  $z$ -directions are fully uncoupled and hence, independent two-dimensional phase-space plots can be considered for each of the three coordinates.

secular motion from the “ripple” motion at the rf drive frequency. This latter motion is disregarded and the ion is assumed to be moving in a harmonic three-dimensional time-independent potential:

$$\Phi(z) = \frac{eV_{0-p}}{mr_0^4\Omega^2}z^2 \quad (4)$$

$$\Phi(r) = \frac{eV_{0-p}}{4mr_0^4\Omega^2}r^2$$

Using Eqs. (2) and (4) and applying Newton’s second law to a harmonic oscillator:

$$m \frac{d^2u}{dt^2} = -eE_u = -e \frac{d\Phi(u)}{du} = -\omega_u^2 u \quad (5)$$

one may express the secular frequencies  $\omega_u$  in both radial and axial directions in terms of the stability parameter  $q_u$ . In general (when  $U \neq 0$ ),  $\omega_0$  can be obtained using the Dehmelt approximation  $\omega_0^2 \approx (a + q^2/2)\Omega^2/4$  [19]. Note that  $a$  and  $q$  are dimensionless parameters.

### 3. Experimental

Experiments are carried out in a quadrupole ion trap (R.M. Jordan Co.) operated in mode II [2], i.e.,

the rf voltage is applied to the ring electrode and there is no dc potential between the ring and the endcap electrodes. The entire trap is biased at a positive dc potential, to allow for extraction of cations into a time-of-flight spectrometer with the detector at ground potential. The TOF mass spectrometer is equipped with a reflectron, which gives near unit resolution at typical ion masses studied here. Ions are pulse extracted through a 3-mm diameter hole in one of the endcaps. An impression of the experimental apparatus is given in Fig. 2. It should be noted here that additional experiments have been performed in a linear TOF set-up (i.e., without reflectron) where similar observations are made and thus, the time dependence of ion signals described in the next sections is considered to be exclusively due to the ion trap.

There is no dc potential between ring and endcap electrodes and therefore the stability  $a$ -parameter is zero. The rf frequency  $\Omega$  is fixed at 1 MHz and the inner radius of the ring  $r_0$  is 1 cm. Using these data and Eq. (2) one can write the stability  $q$  parameter in axial and radial direction as

$$q_z = -2q_r = 0.097 \frac{V_{0-p}}{m} \quad (6)$$

where  $m$  is in amu and  $V_{0-p}$  in V.

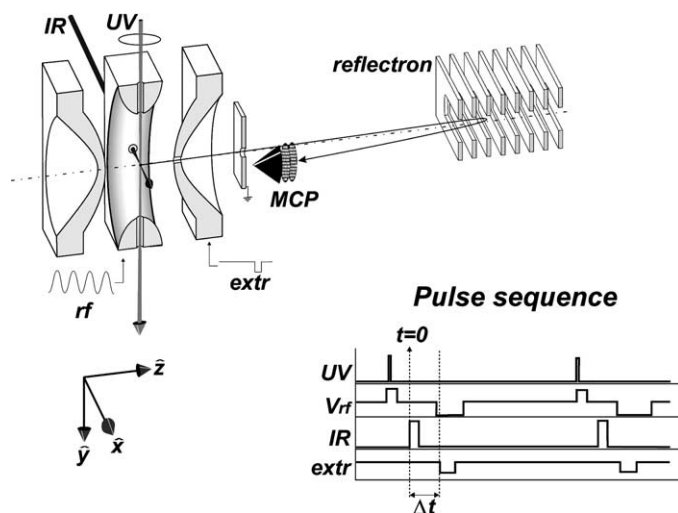


Fig. 2. Schematic of the experimental set-up showing (a cut through) the quadrupole ion trap, the UV and IR laser beams and the reflectron TOF mass spectrometer. Note that the size of the trap has been exaggerated. The timing scheme of the experiment is sketched in the diagram:  $t = 0$  is defined at the moment of IR dissociation, i.e., creation of the fragments, and the extraction time delay  $\Delta t$  is scanned.

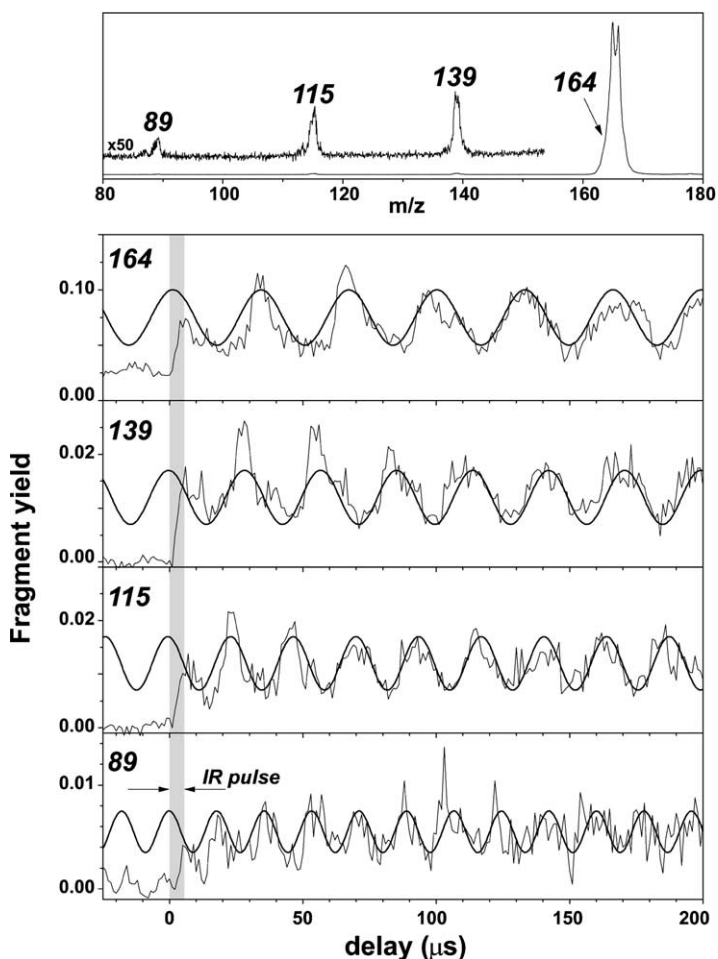


Fig. 3. Mass spectrum of fluorene with the dissociation laser at  $\lambda = 6.5 \mu\text{m}$  (upper panel) and fragment yields on mass channels 164, 139, 115 and 89 as a function of the time delay between fragmentation and extraction (lower panels). The sinusoidal fit to Eq. (7) is given by the thick line. The infrared laser pulse, fired at  $t = 0$ , is indicated by the shaded area.

A sample of fluorene ( $\text{C}_{13}\text{H}_{10}$ ) is placed inside the vacuum chamber and the vapor pressure at room temperature is sufficient to perform the measurements. An ArF excimer laser is focused in the center of the trap to ionize the fluorene molecules, which are instantaneously trapped. UV-induced fragments are removed from the trap by temporarily (2 ms) increasing the rf amplitude as sketched in the timing sequence diagram in Fig. 2. During this pulse, the rf amplitude is chosen such to cause mass selective instability, and hence axial ejection, of all species with  $m < 166$ . After 3 ms (we shall define this moment as  $t = 0$ ), an intense

infrared pulse from the free electron laser “FELIX”<sup>2</sup> is fired at the ion cloud. The wavelength of FELIX is tuned to  $6.5 \mu\text{m}$ , which corresponds to a strong absorption in the fluorene ion [21], thus inducing multiphoton absorption leading to dissociation. The IR pulse duration amounts to about  $5 \mu\text{s}$ , which corresponds to five rf cycles of the ion trap, and the IR laser pulse is not synchronized to the rf phase. After a variable

<sup>2</sup> The free electron laser for infrared experiments (FELIX) delivers IR pulses in the wavelength range  $5\text{--}250 \mu\text{m}$ . The pulse length is approximately  $5 \mu\text{s}$  and the energy is around 50 mJ per pulse. For details see Ref. [20].

delay (see Fig. 2), ions in the trap are pulse extracted and mass analyzed in the reflectron TOF spectrometer. During extraction, the rf voltage on the ring electrode is switched off. The transient from the microchannel plate (MCP) detector is captured and averaged ( $32\times$ ) by a digital oscilloscope (Yokogawa DL4200). Various fragmentation channels exist as can be seen in the upper panel of Fig. 3; main fragments are observed at masses 164, 139, 115 and 89 amu, corresponding to the loss of  $\text{H}_2$ ,  $\text{C}_2\text{H}_3$ ,  $\text{C}_4\text{H}_5$  and  $\text{C}_6\text{H}_5$ , respectively.

For the analysis of the observed effects described in the following it is important to note that (1) the timing sequence of laser pulses and extraction is not synchronized with the rf phase, and (2) the duration of the fragmentation laser pulse ( $5\ \mu\text{s}$ ) in comparison with the 1 MHz rf frequency should cause any effects of the micromotion to smear out. Despite these two arguments, very clear coherences in the ion signals are observed as presented in the next section.

## 4. Experimental results

### 4.1. Experiment 1: oscillation of ion signal intensity

In the first experiment, the extraction time is scanned from  $25\ \mu\text{s}$  before the IR pulse to  $200\ \mu\text{s}$  after the IR pulse in  $1\text{-}\mu\text{s}$  steps, and the intensity in the fragment channels is monitored.

The intensity in all fragment channels oscillates with extraction time as is shown in Fig. 3. As seen from the  $m/T$  column in Table 1, the oscillation period is proportional to the mass of the fragment to within 2%. Therefore, we likely see an effect of the secular ion motion because for  $q_z \leq 0.4$  one finds that  $\omega_0 \propto$

$q_z \propto 1/m$ . In addition, from extrapolation to  $t = 0$  one notices that at the time point where the fragments are formed, all signals are in phase at the maximum intensity. As shown in Fig. 3, the observed fragment yields ( $Y$ ) on the different mass channels are empirically fitted to a sinusoidal function superimposed on a constant offset  $B$ :

$$Y = B + A \sin(\omega t + \phi) \quad (7)$$

and the fitted frequency ( $\omega/2\pi$ ) as well as the modulation depth, defined as  $2A/(A+B)$ , are given in Table 1.

The observations are compared to the calculated secular frequencies using Eq. (6) and the Dehmelt approximation. Comparing observed frequencies of the signal intensity oscillations with calculated frequencies for the secular motion in the axial ( $z$ ) direction in Table 1 (and correcting for an apparent systematic deviation), agreement to within 2.5% is found. Apparently, there is an oscillation in the efficiency with which the ions reach the MCP detector. Clearly, the ions oscillate coherently because otherwise the effect would have smeared out and be unobservable. The oscillation may be due to the axial motion with frequency  $\omega_{0z}$  as is suggested in Table 1, but it is also possible that we see the oscillation in the radial direction at twice the secular frequency  $2\omega_{0r}$  ( $=\omega_{0z}$ ), e.g., when extraction from the trap is more efficient at the extremes (or at the zero-crossings) of the motion.

It is noted that oscillation of the MCP signal intensity is also observed directly after UV ionization, i.e., not using the IR laser (not shown). However, in this case, the signal intensities at the parent ion mass and at the UV-induced fragment masses show more irregular oscillations than those shown in Fig. 3. The strongly oscillating parent ion signal makes it difficult to determine accurate fragment yields. The oscillations dephase after one to a few hundred microseconds so that, in the experiment described here, where the dissociation IR laser is fired 3 ms after the ionization UV laser, dissociation occurs from a steady population of parent ions. This two laser scheme offers an important advantage for these experiments: the UV laser induces only ionization of the neutrals (since UV laser-induced fragments are ejected) and

Table 1  
Observed and calculated oscillation parameters for different fragment masses with  $T$  ( $\mu\text{s}$ ) and  $\omega$  (kHz)

| Observed |      |               |       |       | Calculated |                    |
|----------|------|---------------|-------|-------|------------|--------------------|
| $m$      | $T$  | $\omega/2\pi$ | $m/T$ | Depth | $q_z$      | $\omega_{0z}/2\pi$ |
| 164      | 32.8 | 30.5          | 5.000 | 0.48  | 0.089      | 31.4               |
| 139      | 28.9 | 34.6          | 4.810 | 0.52  | 0.105      | 37.0               |
| 115      | 23.0 | 43.5          | 5.000 | 0.50  | 0.126      | 44.7               |
| 89       | 17.9 | 55.9          | 4.972 | 0.38  | 0.163      | 57.8               |

the IR laser on the other hand only induces fragmentation. Thus, the two processes do not interfere, which greatly simplifies the interpretation.

#### 4.2. Experiment 2: oscillation in the ion arrival time

If one looks in detail at the time of flight (i.e., the arrival time on the MCP detector) for a single mass as function of the delay between fragmentation laser pulse and extraction time from the ion trap, one notices another oscillation. In Fig. 4, subsequent mass traces taken at increasing time delays are shown. The

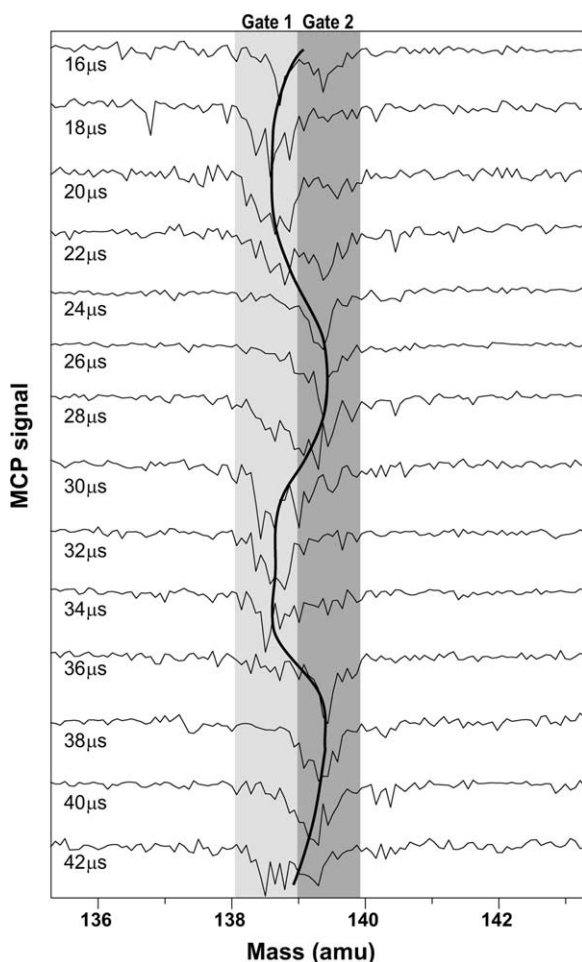


Fig. 4. TOF traces zoomed to fragment mass 139. Oscillation in the exact arrival time is observed as a function of time delay between fragmentation and extraction. The vertical scale of each trace is normalized to remove the intensity oscillations shown in Fig. 3.

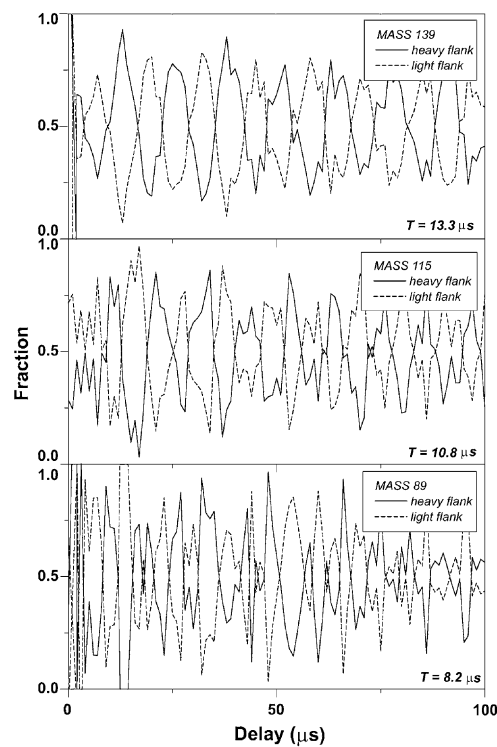


Fig. 5. Integrated signal in lighter and heavier flanks of different mass peaks obtained by setting gates as indicated in Fig. 4.

mass 139 fragment peak is seen to fluctuate around the intrinsic value with an amplitude corresponding to about  $\pm 0.5$  amu. The oscillation can be visualized by setting separate gates over the left and right hand flanks of the mass peak as indicated in Fig. 4. Plotting the integrated intensities in the two gates as function of the time delay, two oscillating traces with  $180^\circ$  phase lag are observed (Fig. 5). Again, the period of oscillation is proportional to the fragment mass ( $m \propto T$ ), suggesting that the oscillation is caused by the ions' secular motion. In addition, it is again clear that the fragmentation laser has induced coherence in the ion motion. However, if we compare this observation to the oscillation in signal intensity described in Experiment 1, we see that the frequency of the oscillation is about two times higher here; comparison of the observed frequency with  $2\omega_{0z}/2\pi$  yields agreement to within 5% (Table 2). Note that in Refs.

Table 2  
Oscillation periods of ion arrival times for different fragment masses ( $T$  in  $\mu\text{s}$  and  $\omega$  in kHz)

| Observed |      |               |       | Calculated          |
|----------|------|---------------|-------|---------------------|
| $m$      | $T$  | $\omega/2\pi$ | $m/T$ | $2\omega_{0z}/2\pi$ |
| 139      | 13.3 | 75.2          | 10.5  | 74.0                |
| 115      | 10.8 | 92.6          | 10.7  | 89.4                |
| 89       | 8.2  | 122.0         | 10.9  | 115.6               |

[7,10], observation of flight time oscillations at once the axial secular frequency ( $\omega_{0z}/2\pi$ ) is reported.

## 5. Trajectory simulations

In order to understand the effects observed here, ion trajectories in the trap were simulated by numerical evaluation of the differential equations of motion in three dimensions (Eq. (1)) using a fourth order Runge–Kutta algorithm. A detailed discussion of various aspects of ion trap trajectory simulation can, e.g., be found in Chapter 6 of Ref. [3] and in Ref. [9]. The simulations applied here assume a perfect quadrupolar geometry (i.e., equations of motion in  $x$ ,  $y$ ,  $z$  are uncoupled) and the absence of ion–neutral and ion–ion interaction (i.e., no ion cooling and no space charge, respectively). An integration step size of  $0.1 \mu\text{s}$  was found to be sufficiently small to reproduce accurately the ion trajectories including the 1 MHz micromotion. However, for the discussion of the observations, the micromotion is unimportant and we can make efficient use of the pseudo-potential formalism.

Since there is a potential minimum at the center of the trap,<sup>3</sup> it is clear that (at least in theory) an ion with no initial velocity or displacement, will experience no force at any time and therefore will be standing still at the center of the trap. In other words, the initial velocity and displacement of an ion at  $t = 0$  determine

<sup>3</sup> More precisely, the quadrupolar potential has a saddle point at the trap center at all times, which however leads to the same conclusion that particles without initial velocity and displacement will not start to move since the gradient of the potential is always zero in all directions. Note that in the approximation of the pseudo-potential (Eq. (4)) there is a true minimum at the center of the trap.

its trajectory. Therefore, we assume that at  $t = 0$  the distribution of parent ions in the trap forms a homogeneous cloud. This implies that oscillations following the ionization laser pulse have faded at the time point where the fragmentation laser is fired, which has been experimentally checked. The size of the cloud may be estimated from an analysis of the pseudo-potential [2] in the trap and assuming that the ions have thermalized in our room temperature trap.<sup>4</sup> At a trapping potential of  $V_{0-p} = 150 \text{ V}$  the parent ions of mass 166 form a cloud with  $r_{\text{max}} \approx 4 \text{ mm}$  and  $z_{\text{max}} \approx 2 \text{ mm}$ .

Since the fragmentation laser is guided through the trap in the radial plane (say along the  $x$ -axis), we assume that at  $t = 0$  fragments are formed in a volume (mm):

$$\begin{aligned} -4 < x < 4 \\ -0.5 < y < 0.5 \\ -0.5 < z < 0.5 \end{aligned} \quad (8)$$

The average velocity in all three directions is assumed to have thermalized and the mean velocity is assumed to be  $\sim 250 \text{ m/s}$ . The simulation is now run with 50 particles having random initial positions and velocities in the range mentioned. The trajectories in  $x$ -,  $y$ - and  $z$ -directions vs. time (0–200  $\mu\text{s}$ ) are plotted in Fig. 6A. Both the radial and axial trajectories show the secular motion and superimposed the 1 MHz ripple due to the micromotion. Similar to some previously reported trajectory simulations [5,9], a clear structure in the secular motion of the various trajectories is observed, especially in  $y$  and  $z$  directions. For instance in the  $y$ -direction, the ion cloud size oscillates between 1 and 5 mm at twice the frequency of the oscillation of the individual particles, i.e., the secular frequency  $\omega_{0y}$ . The effects become even more clear when two-dimensional cuts through the trap are made and the “breathing” ion cloud is viewed in slow motion. Using the data of Fig. 6, video clips of several of these cuts have been prepared, which can be downloaded from our ftp-server [22].

<sup>4</sup> It is not at all certain whether thermalization is complete ( $U_{\text{kin}} + U_{\text{pot}} = (3/2)kT$ ) after 3 ms since we use no buffer gas cooling (background pressure in our chamber is around  $10^{-6} \text{ mbar}$ ). However, we will assume it here for the sake of the argument.

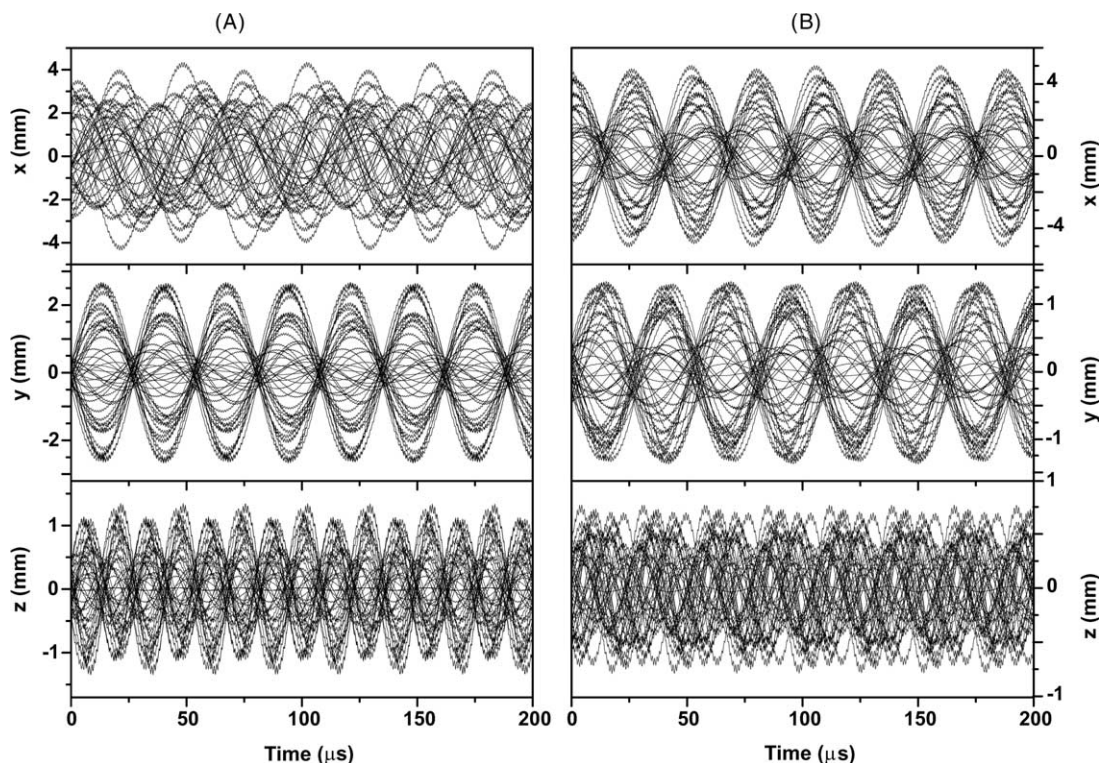


Fig. 6. Simulated ion trajectories for  $m = 139$  amu and  $V_{0-p} = 150$  V. The ions have random initial position and velocity in two different ranges as given in Table 3.

It appears that there is no coherence in the  $x$ -motion, but this critically depends on the ratio between initial velocities and positions. This can be exemplified by assuming slightly different initial conditions (see Table 3), which leads to the trajectories in Fig. 6B, showing coherences in  $x$ - and  $y$ -directions, but not in the  $z$  direction.

Table 3  
Values used in the simulation with mass in amu, frequencies in kHz, positions in mm and velocity in m/s

| Trap parameters             |               |           |         |                    |                    |
|-----------------------------|---------------|-----------|---------|--------------------|--------------------|
| $m$                         | $\Omega/2\pi$ | $V_{0-p}$ | $q_z$   | $\omega_{0z}/2\pi$ | $\omega_{0r}/2\pi$ |
| 139                         | 1000          | 150       | 0.105   | 37                 | 18.5               |
| Range of initial conditions |               |           |         |                    |                    |
|                             | $ x_0 $       | $ y_0 $   | $ z_0 $ | $ v_{0u} $         |                    |
| Fig. 6A                     | 4             | 0.5       | 0.5     | 300                |                    |
| Fig. 6B                     | 5             | 0.5       | 0.5     | 150                |                    |

The phenomenon can be easily understood in terms of the particles' trajectories in phase space, which are obtained by plotting instantaneous velocity vs. position. In this way, the dimension time is eliminated and therefore, the method is only applicable for particles in a time-independent force field. Comparing Eqs. (1) and (4), one finds that opposed to the true quadrupolar potential, the pseudo-potential is indeed time independent. In the pseudo-potential of Eq. (4), a particle's energy is given by

$$U_{\text{pot},x} = -e\Phi(x) = \frac{eV_{0-p}^2}{4mr_0^4\Omega^2}x^2,$$

$$U_{\text{kin},x} = \frac{1}{2}mv_x^2 \tag{9}$$

and similarly for  $y$  and  $z$ . Therefore, by virtue of the harmonic nature of the pseudo-potential, a particle's total energy is proportional to  $\alpha v_x^2 + \beta x^2$ , which

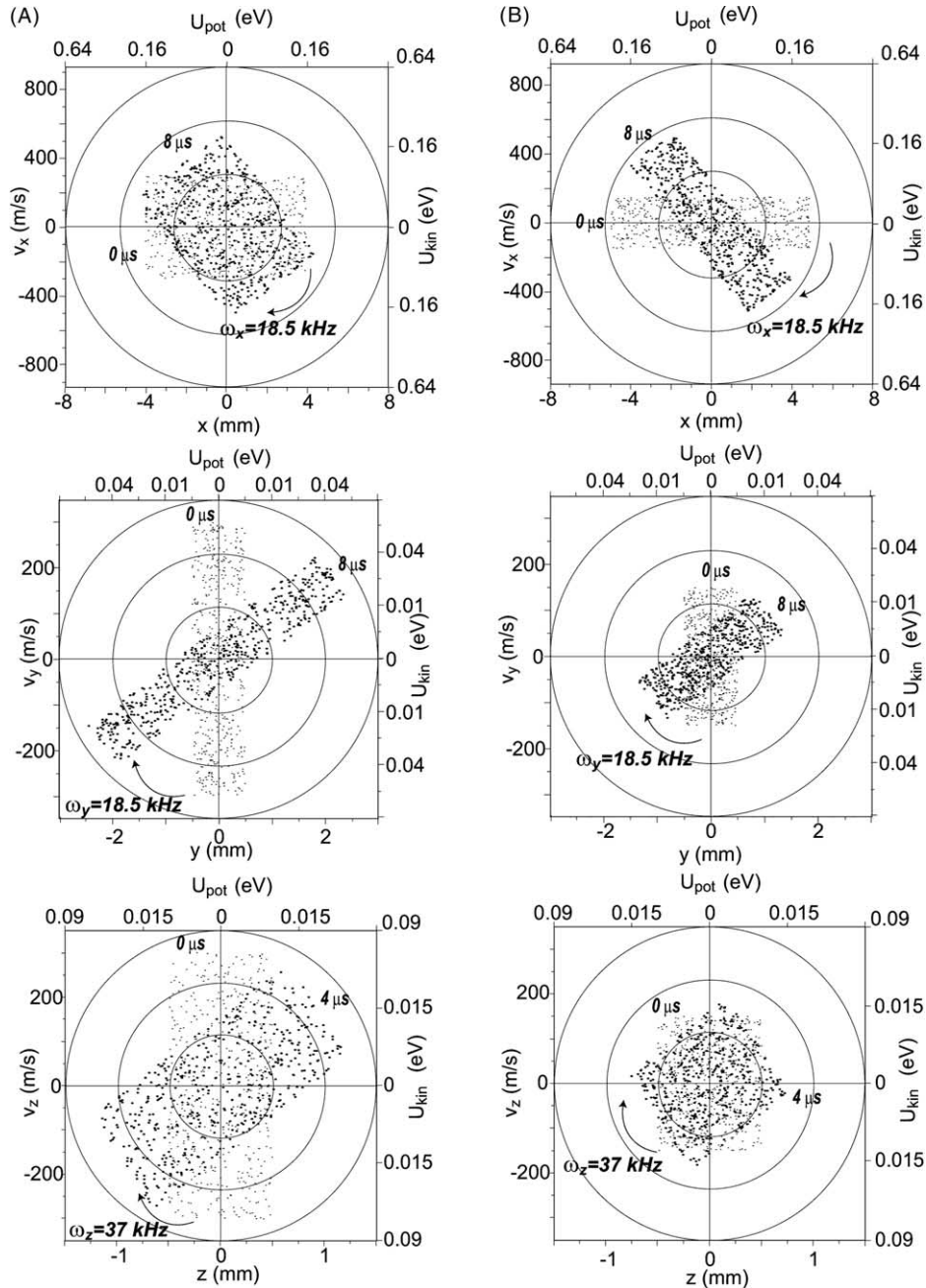


Fig. 7. Phase-space plots along  $x$ -,  $y$ - and  $z$ -coordinates at two different moments in time and for initial conditions A and B (Table 3). The micromotion is suppressed (see Section 5). From a comparison with Fig. 6 it is seen that as the phase-space distribution deviates more from circular, i.e., phase-space matching is less perfect, the real-time distribution shows more breathing. Velocity and position axes are scaled such to represent equal energy spacing so that the iso-energetic lines appear as circles. The scaling is different for radial and axial directions (see Eq. (9)).

yields perfectly elliptic trajectories in the  $x$ - $v_x$  plane. Throughout this work, the horizontal and vertical axes have been scaled such to represent equal energy intervals, so that the iso-energetic lines become perfectly circular. Note that this scaling is different for fragments of different mass, as well as for motion in radial and axial directions (see Eq. (4)), which results in different (secular) frequencies, as is characteristic for a harmonic potential.

Fig. 7 shows the evolution of phase-space distributions of the ion cloud along the  $x$ -,  $y$ - and  $z$ -coordinates corresponding to the real-time trajectories of Fig. 6 (the simulation was now run with 500 ions). After creation of the ion cloud, the distribution starts rotating in phase space, where each particle follows its own iso-energetic path, so that the cloud retains its shape in phase space as seen in Fig. 7. We note here that the influence of the micromotion is suppressed by plotting phase-space distributions always at the same relative rf phase ( $\phi_{rf} = \Omega t/2\pi$ ).<sup>5</sup> The rectangular shapes of the distributions are due to the initial conditions as given in Table 3, which neither include a Gaussian function for the spatial nor for the velocity distribution [12,13,16].

It can be easily verified that the envelope of the cloud in phase space returns to its original position after  $1/2\omega_0$ , half the secular frequency of the individual particles. It is now straightforward to see that the “breathing” motion of the ion cloud as apparent from Fig. 6 results from the “cigar” shape of the ion cloud in phase space. If the cloud would fill up an iso-energetic circle homogeneously, recurrences would not be observable, as is approximately the case along the  $x$  coordinate for initial condition A and along the  $z$  coordinate for condition B. This situation is known as phase space matching [18].

From a further inspection of Figs. 6 and 7, it may be noticed that an initial distribution with larger spread in potential energy than in kinetic energy (see phase-space distribution along the  $x$ -coordinate

in Fig. 7B) leads to a cosine-like behavior in real time (Fig. 6B) and the opposite situation leads to a sine-like behavior (as along the  $y$ -coordinate).

## 6. Discussion

Comparison of observations to the simulated trajectories yields a plausible explanation for the observed oscillations. The oscillations observed in signal intensity (Experiment 1) are likely due to breathing of the ion cloud resulting from a non-circular distribution in phase space. In the radial direction, the orientation of the phase-space distribution shows recurrences at  $2\omega_{0r}/2\pi$ . Possibly, the breathing motion of the ion cloud in the radial direction causes minima and maxima in the extraction efficiency through the 3-mm hole in the endcap nearest to the detector. Let's assume that ions are transmitted through the hole only if their instantaneous position in the radial plane is such that  $\sqrt{x^2(t) + y^2(t)} \leq R$ , where  $R$  is the radius of the hole. The extraction efficiency is then simply obtained from Fig. 6 by counting the number of ions that fulfill the above condition, divided by the total number of ions in the simulation (50). A plot of the extraction efficiency vs. time is shown in Fig. 8, which yields good qualitative agreement with the experimental observations of Fig. 3. The shape of the extraction efficiency curve is seen to depend strongly on the various experimental parameters. Note also that the modulation depth depends strongly on the size of the extraction hole relative to the average radial ion cloud size.

The coherent radial oscillations described here compare very well to those induced by a quadrupolar pulse to the endcaps as reported by Cleven et al. [5]. The simulated radial trajectories in Fig. 6 and in Ref. [5] indeed show a similar structure. It may be noted however that the quadrupolar pulse produces a radially symmetric effect, whereas the laser dissociation described here produces non-uniformity in the  $x$ - $y$  plane.

Similarly, the oscillations observed in the arrival time at the detector may be attributed to phase-space oscillations in the axial direction at  $2\omega_{0z}/2\pi$ . Although it is not quite clear how these oscillations exactly arise,

<sup>5</sup> The ion cloud evolution in phase space has also been visualized as short video animations [22]. Here the micromotion has been included.

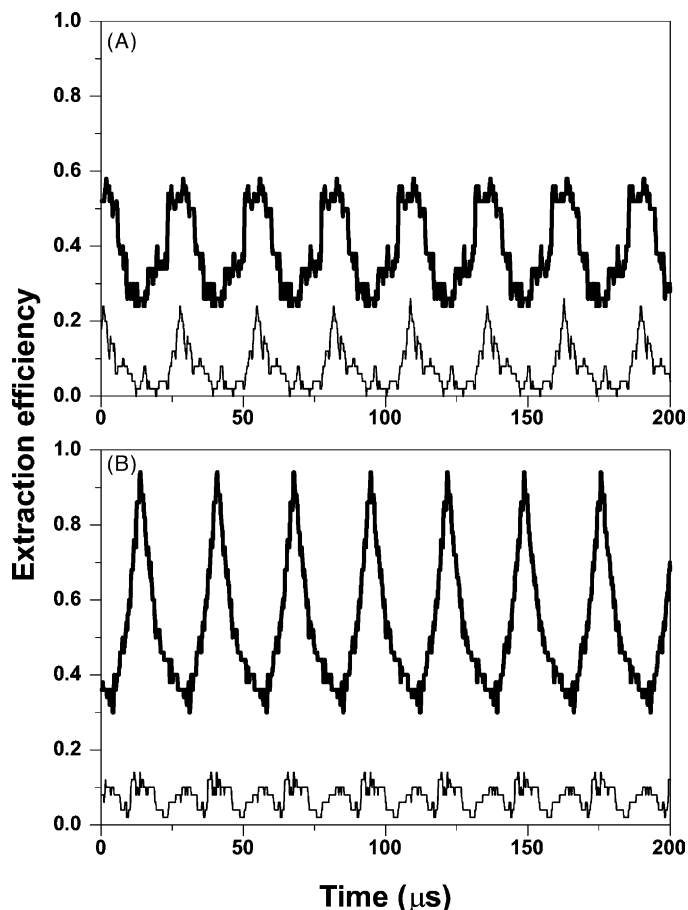


Fig. 8. Computed extraction efficiencies corresponding to the trajectories of Fig. 6A and B. The figure shows that although the individual ions oscillate at their secular frequency  $\omega_r$  in the radial plane, the extraction efficiency is modulated at twice the secular frequency. Substantial differences not only in overall efficiency but also in the shape of the efficiency are found depending on the size of the extraction hole (solid 3 mm, thin 1 mm).

it is likely that they are due to the axial motion of the ions (rather than the radial motion), since the analysis of the phase-space evolution shows that variables are modulated at  $2\omega_0$ . The effect may either be due to spatial breathing of the ion cloud in the axial direction or to the associated periodic variations in the absolute axial velocity of the ions. In contrast to our observations, oscillations in the arrival time at once the axial secular frequency ( $\omega_{0z}/2\pi$ ) were reported by Carette et al. [10]. Moreover, applying their expression for the flight time to the axial trajectories of Fig. 6A, would result in a periodical broadening and narrowing of the

TOF peak, which is not what is observed in our experiment (see Fig. 4). We therefore conclude that the mechanism underlying our observations is different from what is reported in Ref. [10]. For instance, the axial breathing motion may well cause fluctuations in the space focusing characteristics of the ion trap-TOF system. More detailed trajectory calculations including the TOF trajectories are needed to clarify this point.

In Fig. 3, we observe that signal intensities at  $t = 0$  for all fragment masses are in-phase (as expected) and at their maximum as in Fig. 8A as opposed to Fig. 8B. Therefore, one could conclude that at  $t = 0$ , the cloud

has the shape of a cigar stretched along the velocity coordinate. One could then hypothesize that, in this experiment, the energy corresponding to the average initial velocity is larger than that corresponding to the average initial position, i.e.,  $\langle U_{\text{kin}} \rangle > \langle U_{\text{pot}} \rangle$ . This hypothesis can actually be argued to be fairly realistic since, in the  $y$ -direction, the IR laser intersects only a small part of the thermalized ion cloud, so that the average potential energy is significantly smaller than the average kinetic energy associated with the motion in  $y$  direction. This leads to the sine-like breathing of the ion cloud (Fig. 6A) and a cosine-like extraction efficiency (Fig. 8A), as is experimentally observed. Along the  $x$ -axis, the laser intersects the entire thermalized cloud so that phase-space matching occurs. In this situation, an asymmetric distribution of kinetic and potential energies is also induced along the  $z$ -direction (see Fig. 6A), which may lead to the observed oscillations at  $2\omega_{0z}$ , in the detector arrival time.

In some time resolved experiments using ion traps in combination with TOF detection, the oscillations described here may be an unwanted side effect. For instance, in this study it is difficult to determine the fragmentation lifetime from the rising slope of the fragment intensity in Fig. 3. Based on the current findings, a straightforward way to get rid of the oscillations may be buffer gas cooling, as is done in many ion trapping experiments. Buffer gas cooling leads both to smaller initial velocities and positions before the fragmentation laser is fired, as well as to quicker dephasing of oscillations after the fragmentation. In terms of phase space, dephasing will form a homogeneously filled circular ion distribution. However, in those experiments, collisions with buffer gas molecules may interfere with the fragmentation lifetimes under study. In addition, differential pumping is usually required to allow for high enough buffer gas pressures to be applied. One may also consider raising the rf amplitude  $V_{0-p}$ , which makes the potential steeper and thus confines the ions better. Note that this argument assumes that ions have thermalized, which requires buffer gas cooling as well. An additional advantage may be the higher secular frequencies, which cause enhanced dephasing. In the present experiments, a relatively low

rf amplitude was applied as the resolution in the TOF transient deteriorated severely at increasing  $V_{0-p}$ . A simpler solution may be to enlarge the size of the extraction hole such that it is larger than the ion cloud at all times. However, this may not overcome the oscillations in the arrival time at the detector. Obviously, the most elegant solution would be to make use of phase-space matching. For instance, for a given velocity distribution, one could attempt to create a matching spatial distribution, e.g., by adjusting the size and shape of the laser focus.

## 7. Conclusions

Temporal oscillations are observed in signal intensity as well as in arrival time when monitoring laser-induced fragmentation in a quadrupole ion trap equipped with a TOF mass spectrometer. The observations can be well understood with the use of trajectory simulations and considering the motion of the ion cloud in phase space. Key to the observed oscillation of ion signals is the asymmetry in the distribution of initial kinetic and potential energies. This work experimentally shows that such an asymmetry may be created by a focused laser beam interacting with the ion cloud.

The trajectory calculations and the analysis in terms of the evolution of phase-space distribution as presented in this work clearly show that oscillatory behavior can be observed even from a uniform distribution of initial positions and a uniform distribution of initial velocities, if the distribution in phase-space is non-uniform. This is fundamentally different from the experiments of Weil et al. [8], where using pulsed ac excitation an off-axis phase-space distribution is created and released at a random angle, as well as from the experiments of Grottemeyer and coworkers [6,7], where the ion cloud is injected into the trap with a strongly asymmetric velocity distribution. In terms of phase space, these experiments give rise to a bouncing ion cloud (see Fig. 1). The present experiments show that an asymmetry of the average initial positions with respect to the average initial velocities

( $\langle U_{\text{kin}} \rangle$  vs.  $\langle U_{\text{pot}} \rangle$ ) may result in recurrences in the ion signals due to a coherent evolution of the non-circular but on-axis phase-space distribution. This effect can best be compared to the coherent radial oscillations induced by a quadrupolar pulse [5]. The underlying ion dynamics can be described as breathing in phase space. Finally, it may be noted that, in contrast to the bouncing motion, the breathing motion will escape detection when the differential image current between the two endcaps is measured [15].

### Acknowledgements

We greatly appreciate the many discussions with Giel Berden, Hendrick Bethlem, Chava Lifshitz and Stephan Schlemmer during the various stages of this study. This work is part of the research program of FOM, which is financially supported by the Nederlandse Organisatie voor Wetenschappelijk Onderzoek (NWO).

### References

- [1] W. Paul, *Rev. Mod. Phys.* 62 (1990) 531.
- [2] R.E. March, R.J. Hughes, *Quadrupole Storage Mass Spectrometry*, Wiley, New York, 1989.
- [3] R.E. March, J.F.J. Todd, *Practical aspects of ion trap mass spectrometry, Fundamentals of Ion Trap Mass Spectrometry*, vol. I, CRC Press, Boca Raton, 1995.
- [4] J.F.J. Todd, A.D. Penman, *Int. J. Mass Spectrom. Ion Process.* 106 (1991) 1.
- [5] C.D. Cleven, M. Nappi, R.G. Cooks, A.W. Garrett, N.S. Nogar, P.H. Hemberger, *J. Phys. Chem.* 100 (1996) 5205.
- [6] U. Wilhelm, K.P. Aicher, J. Grotemeyer, *Int. J. Mass Spectrom. Ion Process.* 152 (1996) 111.
- [7] U. Wilhelm, C. Weickhardt, J. Grotemeyer, *Rapid Commun. Mass Spectrom.* 10 (1996) 473.
- [8] C. Weil, J.M. Wells, H. Wollnik, R.G. Cooks, *Int. J. Mass Spectrom.* 194 (2000) 225.
- [9] H.P. Reiser, R.K. Julian Jr., R.G. Cooks, *Int. J. Mass Spectrom. Ion Process.* 121 (1992) 49; H.A. Bui, R.G. Cooks, *J. Mass Spectrom.* 33 (1998) 297.
- [10] M. Carette, P. Perrier, Y. Zerega, G. Brincourt, J.C. Payan, J. Andre, *Int. J. Mass Spectrom. Ion Process.* 171 (1997) 253.
- [11] W.R. Plass, *Int. J. Mass Spectrom.* 202 (2000) 175.
- [12] P.H. Hemberger, N.S. Nogar, J.D. Williams, R.G. Cooks, J.E.P. Syka, *Chem. Phys. Lett.* 191 (1992) 405.
- [13] W.R. Plass, L.A. Gill, H.A. Bui, R.G. Cooks, *J. Phys. Chem. A* 104 (2000) 5059.
- [14] A.G. Marshall, C.L. Hendrickson, G.S. Jackson, *Mass Spectrom. Rev.* 17 (1998) 1.
- [15] E.R. Badman, G.E. Patterson, J.M. Wells, R.E. Santini, R.G. Cooks, *J. Mass Spectrom.* 34 (1999) 889.
- [16] C.D. Cleven, R.G. Cooks, A.W. Garrett, N.S. Nogar, P.H. Hemberger, *J. Phys. Chem.* 100 (1996) 40.
- [17] S.M. Michael, B.M. Chien, D.M. Lubman, *Rev. Sci. Instrum.* 63 (1992) 4277.
- [18] S. Humphries Jr., *Charged Particle Beams*, Wiley, New York, 1990 (Chapter 3.7).
- [19] F.G. Major, H.G. Dehmelt, *Phys. Rev.* 170 (1968) 91.
- [20] D. Oepts, A.F.G. van der Meer, P.W. van Amersfoort, *Infrared Phys.* 36 (1995) 297–308, or the FELIX website <http://www.rijnh.nl/molecular-and-laser-physics/felix>.
- [21] J. Oomens, G. Meijer, G. von Helden, *J. Phys. Chem. A* 105 (2001) 8302.
- [22] Video files in AVI format (playable using, e.g., Windows Media Player) can be downloaded from <ftp://rijnh.nl/pub/jos.oomens>.